2018-07

Creating Real-Time Aeroacoustic Sound Effects Using Physically Derived Models

Selfridge, R

10.17743/jaes.2018.0033
Journal of the Audio Engineering Society
Audio Engineering Society

OPEN ACCESS Freely available online

R. Selfridge, D. Moffat, E. J. Avital and J. D. Reiss, "Creating Real-Time Aeroacoustic Sound Effects Using Physically Informed Models,"
J. Audio Eng. Soc., vol. 66, no. 7/8, pp. 594–607, (2018 July/August.).
DOI: https://doi.org/10.17743/jaes.2018.0033

Creating Real-Time Aeroacoustic Sound Effects Using Physically Informed Models

ROD SELFRIDGE, *AES Student Member*, **DAVID MOFFAT,** *AES Student Member*, **ELDAD J AVITAL, AND**
(r.selfridge@qmul.ac.uk) (dj.moffat@qmul.ac.uk) (e.avital@qmul.ac.uk)

JOSHUA D. REISS, *AES Fellow*
(joshua.reiss@qmul.ac.uk)

Queen Mary University of London, Mile End Road, E1 4NS, London, UK

Aeroacoustics is a branch of engineering within fluid dynamics. It encompasses sounds generated by disturbances in air either by an airflow being disturbed by an object or an object moving through air. A number of fundamental sound sources exist depending on the geometry of the interacting objects and the characteristics of the flow. An example of a fundamental aeroacoustic sound source is the Aeolian tone, generated by vortex shedding as air flows around an object. A compact source model of this sound is informed from fluid dynamics principles, operating in real-time, and presenting highly relevant parameters to the user. A swinging sword, Aeolian harp, and propeller are behavior models are presented to illustrate how a taxonomy of real-time aeroacoustic sound synthesis can be achieved through physical informed modeling. Evaluation indicates that the resulting sounds are perceptually as believable as sounds produced by other synthesis methods, while objective evaluations reveal similarities and differences between our models, pre-recorded samples, and those generated by computationally complex offline methods.

0 INTRODUCTION

From the late 19th Century through to the present day, the speed of manmade vehicles and machinery has greatly increased and with that the amount of aeroacoustic noise generated has greatly grown. This has required research into the sounds and noises produced, often in an attempt to minimize noise pollution or structural fatigue [1]. One of the most important developments was in the 1950s and 1960s when Lighthill published his seminal work taking the fundamental fluid dynamics equations, the Navier-Stokes equations, and applying them to the wave equation to predict acoustic sounds [2].

Research into aeroacoustics has often revealed key *semi-empirical* equations enabling the calculation of a number of properties of the tones heard. Semi-empirical equations are ones in which an assumption or generalization has been made to simplify the calculation or yield results in accordance with observations. They allow us to identify key parameters, how they relate to each other and to the sounds generated.

It was shown in [3] that aeroacoustic sounds in low flow speed situations could be modeled by the summation of compact sound sources, namely monopoles, dipoles, and quadrupoles. An acoustic monopole, under ideal conditions, can be described as a pulsating sphere, much smaller than the acoustic wavelength. A dipole, under ideal conditions, is equivalent to two monopoles separated by a small distance but of opposite phase. Quadrupoles are two dipoles separated by a small distance with opposite phases. A longitudinal quadrupole has the dipoles axes in the same line while a lateral quadrupole can be considered as four monopoles at the corners of a rectangle [4].

Many fundamental aeroacoustic sounds can be modeled based on the geometry of objects and the characteristics of the airflow. When air flows over a cavity, a tone is produced either by a fluid dynamic feedback process or resonance within the cavity. The edge tone is created when air leaving an orifice strikes an edge, causing an oscillating feedback to the orifice and generating a tone.

The hole tone is generated when air is forced through a small hole like a kettle whistle and turbulence sounds are created by the vortices themselves. The Aeolian tone is the sound generated as air flows around an object. A simplified tree structure is shown in Fig. 1. A non-exclusive list of sounds that include these aeroacoustic sound sources, either partially or completely, are also shown.

This article presents a real-time sound synthesis model of the Aeolian tone based on a compact sound source. The model was developed to include the tone frequency, acoustic intensity angles, bandwidth, and harmonics.

To illustrate the flexibility and scope of the Aeolian tone compact source synthesis model, three example sounds effect models were developed. A sword was made from a

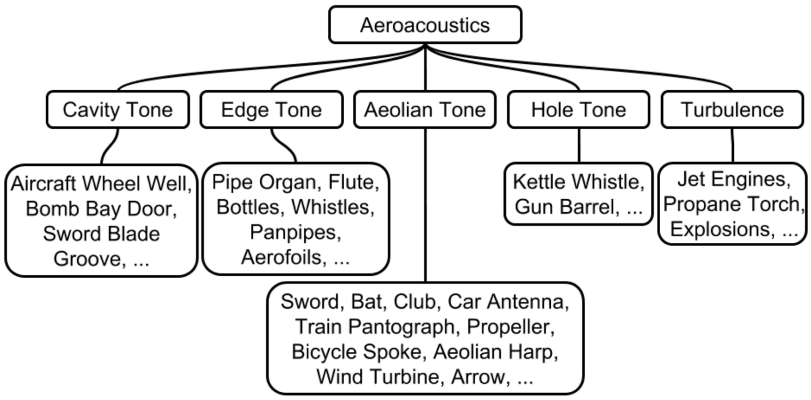

Fig. 1. Simplified taxonomy of fundamental aeroacoustic sounds including examples of each.

number of compact sources; an Aeolian harp to illustrate the interaction between fluid dynamics forces and mechanical properties; and a propeller combining the Aeolian tone source with additional aeroacoustic sounds. Evaluation was carried out for each one to measure the accuracy and plausibility when compared to real samples and other synthesis techniques.

The sound synthesis models presented have great potential for use in nonlinear media such as virtual reality and video games. Live performance, films or television post production can also benefit from our bespoke effects. The synthesis models are classified as *Procedural Audio* sound effects, described in [5] as, "nonlinear, often synthetic sound, created in real time according to a set of programmatic rules and live input." In our models, each sound was uniquely produced based on the current situation, i.e., speed of air/object motion, object dimensions, observer or camera position, etc. Parameters can be manipulated by a user or fully automated by a game engine, producing instant changes in real-time.

This article is a revised and extended version of a paper presented at the 141st Audio Engineering Society Convention [6] that won the best paper award and is organized as follows. Background to the topic, including current state of the art, is given in Sec. 1. Sec. 2 presents the fluid dynamics behind the Aeolian tone and semi-empirical equations used to predict the sounds. Implementation of these findings is described in Sec. 3, and evaluation results in Sec. 4. A number of different synthesis models based on the Aeolian tone are given in Sec. 5, including their evaluation. A final discussion is presented in Sec. 6.

1 BACKGROUND AND RELATED WORK

Sound effects are commonly used in virtual reality, games, films, and television. They can be *samples*, real recordings of the naturally occurring sounds, *Foley*, sounds specifically performed for added emphasis [12], and *synthesized*, sounds generated, usually mathematically, to replicate the effects. Sample clips are usually of high quality but have the drawback that they are identical each time they are played. In a virtual reality or game environment this repetitiveness has the potential to diminish authenticity and increase listener fatigue. A procedural audio sound synthesis model can overcome this problem by adapting the sound to nuances in each new circumstance, although more perceptual evaluation on how users interact and perceive these is required [13].

There are a number of techniques that can be used for sound synthesis whether that be for sound effects, musical instruments, speech or sound textures. Usually these are either based on abstract signal-based techniques or physical models. Signal-based synthesis techniques are often computationally compact but have a significant drawback when deciding how to parameterize the models and control strategies. Physical models often are more computational, some techniques requiring specialized hardware to obtain real-time performance.

Signal-based techniques are based on the perceptual or mathematical content of the sound signals and includes additive synthesis, noise shaping, AM, FM, granular, and wavetable. Additive synthesis is based adding together partials from the Fourier series of a signal to replicate a sound. Practically there is a limitation on the number of partials that are used and often this results in a synthetic sound. A modified additive synthesis method for a trumpet is presented in [14] that uses a source filter model to add in-harmonic partials to achieve a more natural sound.

Noise shaping starts with a source with a wide spectrum, often white noise, and shapes the spectrum to achieve the desired sound. A number of environmental sound textures are presented in [8] using this technique, including the sound of winds that are similar to our model. Sound effects from engines to winds are presented in [7] in which noise shaping is the fundamental technique. The whistling wind sounds presented in [7] is again similar to our model.

In [11] a sword sound effect is presented using granular synthesis. This is where a number of sound atoms or grains are combined to produce the desired signal. Related to this is concatenative synthesis where the clips are longer and individually recognizable. Concatenative synthesis for sound effects has found success with the concept of pre-computed sound textures selected on real-time analysis of animations [15]. The real-time crumpling paper sound effects in [16] is an example of this technique.

Wavetable synthesis is when a waveform is stored in a buffer and the sampling frequency varied to achieve the desired pitch. Aliasing can be an issue with this method and techniques like integrating the wavetable samples can reduce this [17].

Similar to signal-based methods, there are a number of techniques that are described as physical models, including model synthesis, digital waveguide, and numerical solutions. Three points that are considered paramount when designing a physical model are given in [18]. These are that the instrument is studied carefully, properties of the human auditory system are considered to judge if the sound is satisfactory or not, and the model should be computable in real-time.

Model synthesis is similar to additive where the vibrations of resonant structure and the interactions between structures are simulated [19]. Finite element analysis is one method for computing the vibration modes. Modal synthesis for musical instruments is described in [20], which can be extended to contact forces [21] and bubble/water sounds [22].

A common and successful technique for physical modeling is by the use of digital waveguides as initially illustrated by [23]. This has been extended to include fractional delay lines, body modeling, estimation of parameters, and methods of control for a number of plucked stringed instruments in [18]. A flute sound is synthesized in [24] where a digital waveguide was used to capture the most relevant physical characteristics while signal-based analysis / synthesis techniques were used to capture perceptual effects. To capture the unusually wide vibrato effect of a Korean geomungo [25] used a time-varying loss filter.

An alternative method of physical modeling is to discretize a space and time representation of the physical object, most often used for musical instruments; [26] for strings and [27–29] for flue instruments. These techniques do not depend on specific assumptions and are appropriate for nonlinear problems. As well as musical instruments and sound effects, the finite-difference time-domain has been shown to be a suitable method for modeling room acoustics [30].

The numerical solutions obtained in [27–29] were computationally complex; the author states that with their current computing resources one second of sound would take several months of calculation [29]. Perceptual evaluation of these methods has not been carried out for any of these models.

A physical model sound effect of a sword swing was presented in [10] where computational fluid dynamics (CFD) software using a finite difference method provided a numerical solution to the fundamental Navier-Stokes equations. Due to the complexity of these calculations sound textures had to be pre-computed and the speed of playback was varied in real-time in accordance with the speed of the sword.

To contend with the complexity of numerical methods and long processing time the use of specialized parallel processors has been investigated to optimize the computations towards real-time operation. Graphical processing units (GPU) were used in [31] for three-dimensional simulation of a timpani. Real-time synthesis from two-dimensional simulations of a trumpet, clarinet, and flute using a GPU were presented in [32], extending to experimental instrument designs. This was extended to speech synthesis in [33]. Similarly, field programmable gate arrays (FPGA) have also been used for acoustic modeling [34] and modeling musical instruments [35], achieving real-time performance.

When signal-based models introduce aspects of the physical processes into the control of the models they are known as *physically inspired*. Both [7] and [8] varied the center frequency of a bandpass filter in sympathy with the change in airspeed in their wind models. Although tone pitches do increase with airspeed there are other parameters that also contribute to the tone frequency that these models do not consider. The airspeed can also affect other aspects of the sound, like gain, which again were not considered.

We present a physically informed model of an Aeolian tone. A number of different approaches to synthesizing sounds based on the Aeolian tone, including our model, is given in Table 1. Unlike numerical methods, we do not discretize space and time to simulate the fundamental Navier-Stokes equations for finite components, iterating over time. Likewise, the physics of this problem does not lend itself to digital waveguides, which are more suited to resonant vibrations within strings and tubes.

Our implementation is based upon semi-empirical equations, experimental observations, and fundamental aeroacoustic definitions (Sec. 2). We thereafter adopted an abstract synthesis technique to implement the model (Sec. 3), obtaining the benefits of the low computational requirements of these methods and real-time performance. To assess the accuracy of the frequency prediction of the equations and experimental observations used to design the model, results are compared to two-dimensional numerical simulations from offline CFD software (Sec. 4).

A number of behavior models using the Aeolian tone synthesis model are presented in Sec. 5 where perceptual evaluations were carried out to ascertain the plausibility of the sound effects. A discussion of the sound effect models, assumptions, and generalization of the aeroacoustic calculations along with areas for future development is given in Sec. 6.

2 AEOLIAN TONE FLUID DYNAMICS

The Aeolian tone is one of the fundamental aeroacoustic sounds created as air flows around an object. Examples include the whistle when wind blows air around a telegraph wire or the swoosh as a sword sweeps through the air. The fluid dynamics of the Aeolian tone is still an area of focus. In our research we identify semi-empirical equations allowing calculation of the fundamental frequencies, the gain relative to observer position, as well as tone bandwidth and harmonic content. Once the parameters were calculated we processed a noise source with standard signal processing filters and gains to produce a single compact sound source of the Aeolian tone. A diagram indicating the coordinates and parameters used throughout is shown in Fig. 2.

Table 1. Comparison of different Aeolian tone (or similar) synthesis where d = diameter, r = scalar distance, θ = elevation angle, φ = azimuth angle, u = airspeed, and b = cylinder length.

Effect	Control	Method	Computation	Physics Used	Assumptions	Reference
Compact Source	d, r, θ, φ , u, b	Physically Informed		Semi-empirical equations	See Sec. 3	Proposed method
	Proof of concept	Noise shaping	Real-time	Filter center frequency & gain $\propto u$	Parameter ratios, uniform radiation & single tone	[7]
Wind	u			Filter center frequency $\propto u$	Pre-set values for wind type	[8]
	u, d, & boundary conditions	CFD	Offline	Euler equations	None	[9]
Sword	Speed of motion		Offline / Real-time	Navier Stokes equations and Curle's method	None	[10]
		Modal Synthesis	Offline / Real-time	Mode amplitude $\propto$ acceleration	Frequency modes fixed	[11]

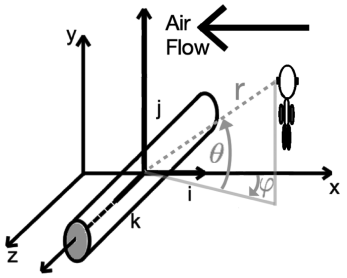

Fig. 2. Coordinate system used for sound emission from a cylinder.

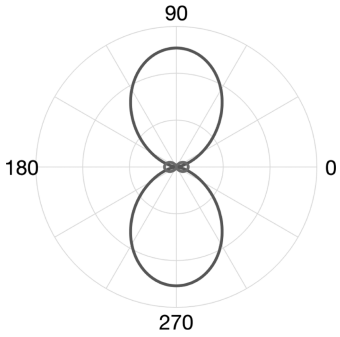

Fig. 3. Ideal radiation patterns for perpendicular dipole sources

2.1 Tone Frequency

In 1878 Czech physicist Vincenc Strouhal carried out one of the first important studies into the frequency of a tone produced as air flows around a cylinder. He defined the formula given in Eq. (1):

$$S_t = \frac{f\,d}{u} \tag{1}$$

where S_t is the Strouhal number, f is the tone frequency, d the cylinder diameter, and u the airspeed.

As air passes a cylinder, vortices are shed from opposite sides at the given frequency. The vortex shedding causes a fluctuating lift force dominated by a fundamental frequency f_l with $S_t \approx 0.2$. Simultaneously, a side axial drag force is present as air flows round the cylinder and its fluctuations are dominated by f_d with $S_t \approx 0.4$. In [36] it was noted that the amplitude of this drag force is approximately one-tenth the amplitude of the lift force.

Aeolian tones can be represented by dipole compact sound sources. There are separate dipoles for the lift and drag fundamental frequencies, as well as for lift and drag harmonics. The acoustic output for ideal lift and drag dipole sources is illustrated in Fig. 3. It can be seen that the major sound source is the lift dipole that is perpendicular to the flow direction. The drag dipole is parallel to the flow direction and has a much smaller influence on the final sound.

The generated sound is strongly influenced by the turbulence created as air flows past the cylinder; the more turbulent the flow, the more diffused the vortices will be. Turbulence is indicated by the dimensionless Reynolds number R_e given by Eq. (2):

$$R_e = \frac{\rho_{air}\,d\,u}{\mu_{air}} \tag{2}$$

where ρ_{air} and μ_{air} are the mass density and dynamic viscosity of air respectively.

An experimental study of the relationship between fundamental Strouhal number associated with the lift force and Reynolds number was performed in [37], giving the following relationship:

$$S_t = \lambda + \frac{\tau}{\sqrt{R_e}} \tag{3}$$

where λ and τ are constants given in Table 2. The different values represent the transition regions of the flow, starting at laminar up to sub-critical turbulence. When the Reynolds number lies between $2\text{x}10^5$ and $1.0\text{x}10^6$ it enters its *Critical* region. Here the Strouhal number jumps to values of approximately 0.45 [38]. Above this region it returns to values similar to the subcritical region, $S_t \sim 0.2$. No values were published for this region in [37].

Using Eq. (2) we calculated the Reynolds number, enabling us to identify values of λ and τ from Table 2. It was

Table 2. Values for constants in Eq. (3), reproduced from [37]. † Linear interpolation between published values. ‡ interpolated from [38].

R_e range	λ	τ
[47,180)	0.2684	–1.0356
[180, 230)	0.2437	−0.8607
[230, 240)	0.4291	−3.6735
[240, 360)	0.2492 †	−0.8861†
[360, 1300)	0.2257	−0.4402
[1300, 5000)	0.2040	+0.3364
[5000, 2x10^5)	0.1776	+2.2023
[2x10^5, 1x10^6)	0.5760‡	−175.956‡

then possible to calculate a value for S_t from Eq. (3) and thereafter the fundamental frequency of the Aeolian tone, Eq. (1). The fundamental lift dipole frequency f_l is given by:

$$f_l = \frac{S_t u}{d} = \left[\lambda + \frac{\tau}{\sqrt{R_e}}\right]\frac{u}{d} \tag{4}$$

and for the fundamental drag dipole frequency f_d:

$$f_d = \frac{2S_t u}{d} = 2\left[\lambda + \frac{\tau}{\sqrt{R_e}}\right]\frac{u}{d} \tag{5}$$

2.2 Source Gain

The time-averaged Acoustic Intensity $\overline{I_{1l}}$ (W/m^2) of the Aeolian tone lift dipole source was derived from Lighthill's acoustic analogy equations [2] via the Ffowcs Williams-Hawkings equation [39] by Goldstein in [40]. Assumptions include that the listener is in the far field (distant from the source where the sound particle velocity is in phase with the sound pressure) and that the dipole source is much greater than the quadrupole. The full derivation is beyond the scope of this article and the reader is referred to [40]. The Acoustic Intensity $\overline{I_{1l}}$ is given by:

$$\overline{I_{l1}} \sim \frac{\sqrt{2\pi}\kappa^2 S_t^2 l\ b\ \rho_{air}\ u^6 \sin^2\theta\cos^2\varphi}{32c^3 r^2(1 - M\cos\theta)^4} \times \left\{exp\left[-\frac{1}{2}\left(\frac{2\pi M\ S_t\ l}{d}\right)^2 \sin^2\theta\sin^2\varphi\right]\right\} \tag{6}$$

where b is the cylinder length, θ is the elevation angle, φ the azimuth angle, c the speed of sound, and r the scalar distance between source and observer (Fig. 2). κ is a numerical constant that lies somewhere between 0.5 and 2.

It was suggested that the sensitivity of κ may be due to turbulence in the oncoming air [40]. M is the Mach number given by $M = u/c$. The correlation length l, has dimensionless units of diameter d and indicates the spanwise length that the vortex shedding is perfectly correlated but random with respect to points outside [41].

We time average the acoustic intensity I in order to account only for the component that propagates to the far field, i.e., pressure decays as $1/r$. If we do not time average I and do the sound measurements in the near field we will also account for "hydrodynamic" pressure components that decay exponentially with r and thus will have negligible presence in the far-field.

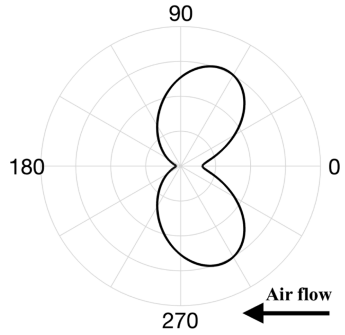

Fig. 4. Composite acoustic intensities of lift, drag, and wake of a single compact sound source varying with elevation θ. $M = 0.2$, azimuth $\phi = 0$. (The airflow direction is from 0° to 180°)

The averaging time period T was given in [40] as:

$$T = \frac{2\pi}{f_l}(1 - M\cos\theta) \tag{7}$$

The sound intensity depends on the airspeed, airflow direction, and listener position. The peak angle of acoustic intensity for the lift dipole is affected by the flow Mach number M; the higher the Mach number, the more upstream the peak. Fig. 4 shows a representation of the resultant acoustic intensity pattern from combining the fundamental sources.

2.3 Harmonic Content

The presence of harmonics in the Aeolian tone is confirmed in [38]. There are two harmonics relating to the lift dipole at $3f_l$ and $5f_l$ with normalized gains of 0.6 and 0.1 of the fundamental respectively [42].

2.4 Tone Bandwidth

The bandwidth around the fundamental frequency is affected by the Reynolds number [43]. Data published in [43] for a range of Reynolds numbers from 0 to 237,000 indicated that the higher the Reynolds number, the wider the tone bandwidth.

2.5 Wake Noise

When the Reynolds number increases the vortices produced by shedding diffuse rapidly, merging into a turbulent wake. The wake produces wide band noise modeled by lateral quadrupole sources whose intensity varies with the power of 8 [41].

There is very little noise content below the lift dipole fundamental frequency f_l [41]. Above this frequency the roll off of the turbulent noise amplitude is $\frac{1}{f^2}$ [44].

The sound generated by jet turbulence was examined in [40, 45, 46]. [40] stated the radiated sound pattern is greatly influenced by a "Doppler factor" of $(1 - Mcos\theta)^{-5}$. The wake noise has less energy than a jet and its intensity $\overline{I_w(t)}$ has been approximated by the authors to capture this

relationship as shown in Eq. (8):

$$\overline{I_w} \sim \Gamma \frac{\sqrt{2\pi}\kappa^2 S_t^2 l b \rho_{air} u^8}{16\pi^2 c^5 (1 - M\cos(\pi - \theta))^5 r^2} \times \left(1 + B\cos^4(\theta) - \frac{B+3}{4}\sin^2(2\theta)\sin^2(\varphi)\right) \quad (8)$$

where Γ is a scaling factor between wake noise and lift dipole noise. No relationship between the two sound sources has been identified and this value was set perceptually (Sec. 3.5). B is an empirical constant, $B \in [-1, 3]$ [45]. The range in the value of B accounts for the possible range of combinations between the various longitudinal and lateral quadrupoles. The value of π was included in the denominator of the first component as the Aeolian tone and wake derivations in [40] were made with the airflow in opposing directions.

3 IMPLEMENTATION OF AEOLIAN TONE

Our model was realized in Pure Data, a real-time graphical data flow programming language. This was chosen due to the open source nature of the code and ease of repeatability rather than high performance computations. The parameters u, d, θ, φ, b, and r were all sampled at audio rate, giving discrete values, $u[n]$, $d[n]$, $\theta[n]$, $\varphi[n]$, $b[n]$, and $r[n]$ where n is the discrete sample number. Being able to vary these parameters at audio rate allows real-time operation of the models.

3.1 Fundamental Frequency Calculation

The Reynolds number R_e was calculated from Eq. (2) using discrete values for $u[n]$ and $d[n]$. Using Table 2, values for λ and τ were identified. Thereafter, the lift fundamental frequency f_l was obtained from Eq. (4) and the drag fundamental frequency from Eq. (5).

3.2 Gain Calculations

The time-averaged intensity value $\overline{I_{l1}}$ calculated by Eq. (6) relates to the dipole associated with the fundamental lift frequency f_l. Previous theoretical research [47] set the constant $\kappa = 1$ and neglected the exponent. [40] confirms that for low Mach numbers the exponent can be neglected. We set $\kappa = 1$ and neglect the exponent, matching conditions used by [47] (see Sec. 6).

The correlation length l values range from $17d$ to $3d$ [47] depending on Reynolds number. A plot showing similar values was given in [48], which highlighted variation between studies but denoted the overall trend of decreasing correlation length with increasing Reynolds number. Taking points from the plot given in [48] enabled the authors to derive an equation replicating the fundamental relationship given in the plot. Due to the variation between results from different studies it is not possible to state an exact error. The equation for l is given in Eq. (9).

$$l = 10^{1.536} R_e^{-0.245} d[n] \quad (9)$$

The intensity value pertaining to the drag force $\overline{I_{d1}}$ was defined by the authors based on Eq. (6) given in [40], with an extra factor of $\frac{\pi}{2}$ added to the numerator elevation angle to account for the 90° phase difference between the lift and drag forces.

$$\overline{I_{d1}} \sim 0.1 \frac{\sqrt{2\pi} S_t^2 b[n] \rho_{air} u[n]^6 l (\sin(\theta[n] + \frac{\pi}{2}))^2 (\cos\varphi[n])^2}{32 c^3 r[n]^2 (1 - M\cos\theta[n])^4} \quad (10)$$

The time averaging period for both Eqs. (6) and (10) was calculated using Eq. (7).

Table 3. Acoustic intensity values for fundamentals and harmonics.

Harmonic	Acoustic Intensity
3 x f_l	$I_{l3} = 10^{0.6 \log_{10} \overline{I_{l1}}}$
5 x f_l	$I_{l5} = 10^{0.1 \log_{10} \overline{I_{l1}}}$
2 x f_d	$I_{d2} = 10^{0.125 \log_{10} \overline{I_{d1}}}$

3.3 Harmonic Content Calculations

A number of harmonics are present in the Aeolian tone (Sec. 2.3). The gain and frequency of the lift and drag dipoles have been calculated, see Table 3. Converting the intensity value to decibels prior to scaling is a revision from [6] and found to be correct with [42]. There are two harmonics relating to the lift dipole at $3f_l$ and $5f_l$. Although a drag dipole harmonics, given in Table 3, was not discussed in [38], they can be observed in the CFD simulations. Thus, the most significant harmonic $2f_d$ was added to our model, although they appear to have little perceptual effect on the resulting sound, see Sec. 4.

3.4 Tone Bandwidth Calculations

As stated in Sec. 2.4, there is a bandwidth around the fundamental frequency and this is related to the Reynolds number. Data available in [43] was limited to Reynolds numbers under 237,000. The relationship between the bandwidth and Reynolds number from 0 to 193,260 was found to be linear. This relationship was interpolated from the data as:

$$\frac{\Delta f_l}{f_l}(\%) = 4.624 \times 10^{-5} R_e + 0.9797 \quad (11)$$

where Δf_l is the tone bandwidth at –3 dB of the lift dipole frequency. Above a Reynolds number of 193,260 a quadratic formula was found to fit the bandwidth data. This is shown in Eq. (12).

$$\frac{\Delta f_l}{f_l}(\%) = 1.27 \times 10^{-10} R_e^2 - 8.552 \times 10^{-5} R_e + 16.5 \quad (12)$$

In signal processing, the relationship between the peak frequency and bandwidth is called the Q value ($Q = f_l/\Delta f_l$), the reciprocal of the percentage value, obtained from Eqs. (11) and (12).

3.5 Wake Calculations

A noise profile of $\frac{1}{f^2}$ is known as *Brown Noise*. This was approximated using white noise and the transfer function shown in Eq. (13) [49].

$$H_{brown}(z) = \frac{1}{1 - \alpha z^{-1}} \tag{13}$$

In [49] α has a value of 1 but this proved unstable in our implementation. A value of 0.99 was chosen, giving a stable implementation while visual inspection did not show any difference in the resulting magnitude spectra. The required noise profile was generated using the transfer function given in Eq. (16):

$$N[z] = H_{brown}[z]W[z] \tag{14}$$

where $W[z]$ is a white noise source and the output $N[z]$ is a brown noise source. There is little wake contribution below the fundamental frequency [41]. Therefore, a high pass filter was applied with the filter cut off set at the lift dipole fundamental frequency, $f_l[n]$. The transform function for the high pass filter $H_{hp}[z]$ is given as:

$$H_{hp}[z] = p^2\left(\frac{1 - 2z^{-1} + z^{-2}}{1 - 2pz^{-1} + p^2z^{-2}}\right) \tag{15}$$

where $p = (1 - 2\pi f_l[n]/f_s)$ and f_s is the sampling frequency, giving a roll-off of ≈35 dB/dec. This produces the turbulent noise profile required, $G[z]$:

$$G[z] = H_{hp}[z]N[z] \tag{16}$$

The inverse Z-transform of $G[z]$ gives the wake output signal, $g[n]$. The wake gain was calculated by Eq. (8). A value of $B = 0.7$ was set in [46] as it was found in [45] to match measured values. No relationship between the intensity for the Aeolian tone dipole sources and for the wake quadrupole sources $\overline{I_w}$ has been identified. A value of $\Gamma = 1\text{x}10^{-4}$, was set perceptually based on the sounds generated from the effects models described in Sec. 5.

3.6 Final Output

To generate the output sound we used a white noise source $W[z]$ filtered by a bandpass filter. The transfer function $H_{bp}[z]$ for the bandpass voltage controlled filter used for all tones is:

$$H_{bp}[z] = \frac{\beta_1 + \beta_2 z^{-1} + \beta_3 z^{-2}}{1 + \alpha_1 z^{-1} + \alpha_2 z^{-2} + \alpha_3 z^{-3} + \alpha_4 z^{-4}} \tag{17}$$

where the coefficient terms for all β and α values are given in terms of f and Q in the Appendix. For the fundamental lift dipole tone the center frequency of the bandpass filter was set to f_l, and the Q value as calculated in Sec. 3.4. The filter output $x_{l1}[n]$ is obtained from the inverse Z-transform of $X_{l1}[z]$ given as:

$$X_{l1}[z] = W[z]H_{bp}[z] \tag{18}$$

The same process was applied in relation to the fundamental drag dipole using f_d as the bandpass filter center frequency with the same Q value used, giving a bandpass filter output $x_{d1}[n]$.

Lift dipole harmonics $3f_l$ and $5f_l$ along with a drag dipole harmonics $2f_d$ were computed in the same way, giving outputs $x_{l3}[n]$, $x_{l5}[n]$, and $x_{d2}[n]$ from their respective bandpass filters.

The gain values for the lift and drag dipole outputs were obtained from Eq. (6) and Eq. (10). The appropriate gain values for the harmonics are given in Table 3. Finally, the wake output $g[n]$ with gain $\overline{I_w}$ was added. Note that a single white noise source was used for all fundamental and harmonic dipoles and for the wake noise as they are all part of the compact source.

Combining the outputs from the lift dipole, drag dipole, harmonics, and wake it is possible to define a final output, Eq. (19).

$$y[n] = \chi\Bigg[\sum_{k=1}^{3}\overline{I_{l(2k-1)}}x_{l(2k-1)}[n] + \sum_{j=1}^{2}\overline{I_{d(j)}}x_{d(j)}[n] + \overline{I_w}g[n]\Bigg] \tag{19}$$

where χ is a user defined gain. It is constant over multiple compact sound sources therefore maintaining the relationships defined by the parameters.

4 AEOLIAN TONE RESULTS

Previous studies have published Aeolian tone frequency values for different airflow speeds and cylinder diameters. The conditions specified in these publications were replicated in our model and the results noted in Table 4.

A number of discrepancies between the published values and values simulated by our model can be seen. This could indicate errors between the equations of our implementation with their built-in assumptions. This could also be due to the wind tunnel experiments being susceptible to noise, for example, from the measurement instruments themselves. Some of the historical measurements date back to the 1950s and 1960s when accuracy of measurement equipment may not have been the same as present day.

To further verify our model, conditions from [51] were replicated using the CFD software, Fluent. This allowed us to note similarities and differences with a commercial package operating offline. In the simulation, we used the Unsteady Reynolds Averaged Navier-Stokes (URANS), equations operating in 2 dimensions. The SST k-ω model was used on a mesh with 73728 elements. The numerical scheme was 2nd order upwind. The velocity vectors for a typical simulation are shown in Fig. 5. The vortex shedding can clearly be seen emerging from the rear of the cylinder.

Acoustic analysis was carried out using the built-in Ffowcs Williams-Hawkings acoustical analysis method [39]. The acoustic receiver was positioned at a distance, $r = 12m$ and an elevation angle, $\varphi = 90^\circ$.

The differences between published results in Table 4 and those obtained from the CFD software were significantly larger than for our model. From the results in Table 4, the average absolute error for our model was 4.66% while CFD has an average absolute error of 18.11%. We can also see

Table 4. Comparison of Aeolian tone frequencies in Hertz; known measured (* read from a graph, ** computed answer), simulated using Fluent CFD and from our synthesis model.

Publication	[50]		[51]	[9]	[52]	[41]		[53]		
Air speed (m/s)	20	40	15	69	69	68.58	42.67	16.6	26.7	32.3
Diameter (m)	0.004	0.004	0.006	0.019	0.019	0.0127	0.0127	0.0254	0.0254	0.0254
Published Frequency	1000	2000*	508	617**	643	1000*	650*	150*	210*	240*
Real-Time Model Frequency	1038	1988	515	674	674	1008	635	125	197	238
% Error	3.8	0.6	1.38	9.24	4.82	0.8	−2.31	−16.67	−6.19	0.83
Fluent CFD Frequency	1113	1635	590	837	837	1148	703	145	245	304
% Error	13.3	−18.25	16.14	35.66	30.17	14.8	8.15	−3.33	16.67	26.67

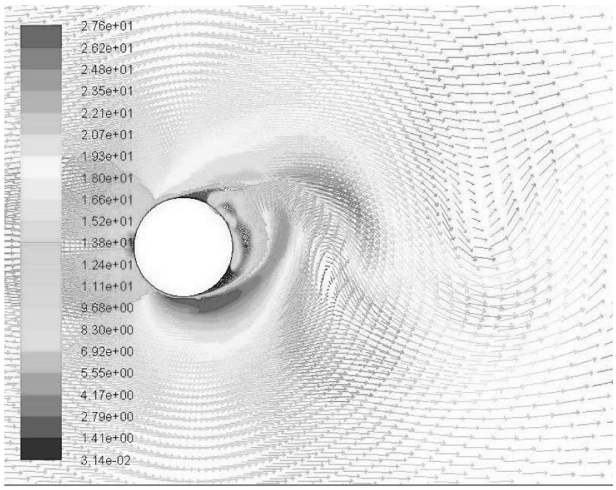

Fig. 5. Velocity vectors showing vortices being shed behind a cylinder.

from the % error values in Table 4 that the CFD calculations consistently overestimate frequency values whereas our model estimates were more equally balanced between less than or greater than published values [50, 51, 9, 52, 41, 53].

There are a number of reasons for these differences, including how the CFD software computes the interaction at the boundary of the cylinder and the main flow domain. Simulating the tones in 2 dimensions means we cannot fully simulate the turbulence which is a 3D phenomenon.

The magnitude spectrum of the Fluent simulation, given in Fig. 6(a), clearly shows the fundamental, 3rd, 5th, and 7th harmonics associated with the oscillating lift force. Peaks can be seen in our model only at the fundamental, 3rd, and 5th harmonics, Fig. 6(b). In Fig. 6(a) there are also peaks at the 2nd, 4th, and 6th harmonics. These are associated with the drag force which have little amplitude at an elevation of 90°. The drag fundamental and 1st harmonic frequencies were generated by our model but were too small to be seen in Fig. 6(b).

An obvious difference in the spectrum produced by the CFD software is that it is virtually a pure tone, along with harmonics. There were no bandwidths as highlighted in [43] because Fluent simulations in 2D are not able to simulate the turbulent structure cascade and just captures tones. The $\frac{1}{f^2}$ roll off will also not be visible.

5 SOUND EFFECT MODELS

In this section we illustrate how the Aeolian tone compact source model can be used entirely or as a component part of sound effects.

5.1 Description of Models

The first model presented is the swinging sword sound effect. A full description of this model was given in [54]. In this model, a number of Aeolian tone sources were placed in a virtual line representing a sword. The air velocity for each source scaled depending on their position on the sword and hence radius of the swing arc. Fig. 7 illustrates the positioning of eight source models on a sword.

The length of the sword, speed of swing, blade thickness, and arc angles can be set by the user or a game engine. A video of the sound effect controlled by the Unity game engine is available[1].

The model was extended to cover a baseball bat and a golf club by adjusting the length and diameters to replicate these objects swinging through the air. A copy of all the sound files used in the perceptual evaluation test and the Pure Data sword demo model are available[2].

An Aeolian harp is a multi-stringed musical instrument, often part of a piece of artwork or sculpture, played by the wind. An example is shown in Fig. 8. In [55] a physical model of the Aeolian harp was presented.

Aeolian tones are generated as the wind blows around each of the strings of the harp. When an Aeolian tone from a string is close to the fundamental vibration frequency, or one of the harmonics, the vortices shed from the string cause the string to vibrate at this vibration frequency. While in this region, the vortex shedding frequency does not vary with the airspeed but remains at the vibration frequency. This region is known as *lock-in* and it is while vibrating at this frequency that an intense sound can be produced. The sound has a profile similar to a frequency modulated tone.

A video giving a further explanation is available[3]. A copy of all the sound files used in the perceptual evaluation test and the Pure Data Aeolian harp demo model are available[4].

[1] https://www.youtube.com/watch?v=zVvNthqKQIk

[2] https://code.soundsoftware.ac.uk/projects/physical-model-of-a-sword-sound

[3] https://www.youtube.com/watch?v=d6c6-u3MQDk

[4] https://code.soundsoftware.ac.uk/projects/aeolianharp

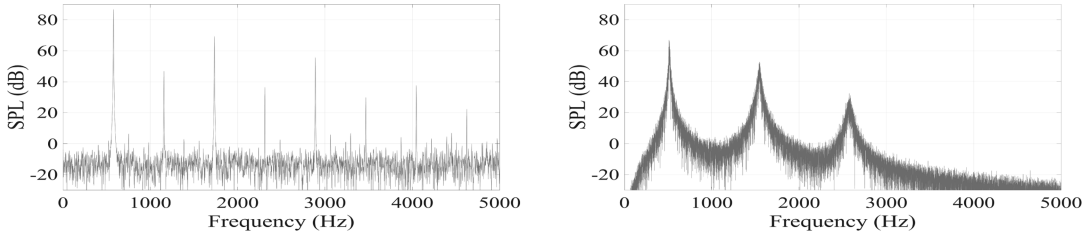

(a) Fluent magnitude response (b) Model magnitude response

Fig. 6. Fluent CFD and our model simulations, $u = 15$ m/s, $d = 0.006$ m.

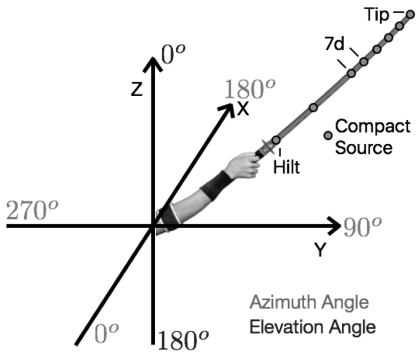

Fig. 7. Position of 8 compact sources and coordinates used in sword model

Fig. 8. Aeolian harp at South Carolina. Picture by Professor Henry Gurr, reproduced by kind permission.

In [56] the sound of a spinning propeller was replicated in a physical model. There are three major sound sources in the propeller model; vortex noise as the blade spins through the air, loading noise due to rotating forces on the blade, and the motor spinning the blades.

The Aeolian tone compact source model was used to replicate the vortex noise in a similar implementation to the sword model. The procedure to predict the loading noise was given in [57]. This allows calculation of the sound pressure level of the fundamental loading frequency and nine harmonics. These calculations take into consideration the RPM of the propeller, engine horse power, azimuth angle of the listener, and spherical attenuation, including air absorption.

The propeller in an airplane is not heard in isolation as calculated above. The motor is often the major sound source. It was not the purpose of our design to replicate the motor component so a model was adapted from the helicopter sound effect in [7]. A number of aircraft and their propellers were replicated to demonstrate the scope and properties of our model, including a Hercules C130, Tiger Moth, and a Cessna 340.

A video of the propeller sound effect mixed into the audio of a movie is available[5] and the sound effect used within a game engine[6]. A copy of all the sound files used in the perceptual evaluation test and the Pure Data propeller demo model are available[7].

5.2 Evaluations

Objective evaluations were carried out on the harp and propeller models where the signal content of examples of each were compared. It is conceded in both objective evaluations that the best test material would be from exact recordings where the physical properties of the harp and propeller are all known, including airspeed. It is possible and of value to examine the characteristics of the sounds produced, comparing characteristics of the output from the physical model to a recorded sample.

For the Aeolian harp model a spectrogram analysis of the output signal indicated that the number of frequency sidebands within the recorded clip was greater than those produced by our model. The number of side bands varied with time, indicating a possible fluid dynamics / mechanics interaction that is not understood nor captured by the synthesis model.

A similar evaluation was carried out on the propeller model using a recorded sample of a Cessna taken from the BBC Sound Effect Library (AircraftCessna.BBC.EC1A4b.wav). Analysis showed that the first peak frequency of the recorded sample was ≈ 80 Hz, corresponding to a two-bladed propeller spinning at 2400 RPM. The physical model was that of a three-bladed pro-

[5]https://www.youtube.com/watch?v=ChZBaKouRGs
[6]https://www.youtube.com/watch?v=h_WX_O1BVds
[7]https://code.soundsoftware.ac.uk/projects/propeller-model

peller spinning at 2200 RPM, which gives the first frequency peak at 100 Hz.

An objective evaluation of the signal identified that there was content not reproduced by the physical model of the propeller. Reasons for this could be due to our model being limited to 10 harmonics for the loading sound, yet many more are present from a real propeller. The motors used for real propellers may produce more wideband noise that the model we have adapted from [7] does not capture. It may also be that more Aeolian tone compact sound sources on the blade would increase authenticity of the vortex sounds produced.

The subjective evaluation for the three sound effect models were performed separately. The physically informed model was evaluated against samples of real recordings of swords, Aeolian harps, and propeller powered airplanes as well as alternative sound synthesis methods. Sounds generated from CFD techniques [10] and granular synthesis [11] were used for the sword sound evaluation and sounds generated from Spectral Modeling Synthesis (SMS) techniques [58] were used to generate synthesized sounds for Aeolian harps and propeller powered airplanes.

A double-blind listening test was carried out to evaluate the effectiveness of our synthesis model. The Web Audio Evaluation Tool [59] was used to build and run listening tests in the browser. This allowed test page order and samples on each page to be randomized. All samples were loudness normalized in accordance with [60]. There was a total of 25 participants for the listening test for the sword sound effect, 32 for the Aeolian harp, and 20 for the propeller.

No training was offered for the sword and propeller sound effects but was for the Aeolian harp sounds. This is because it was believed that participants would have had more exposure to sword and propeller sounds but the Aeolian harp sounds are rarer. As way of training an introductory video was given to all participants to assist them in identifying the Aeolian harp sound[3].

The real-time physical models perform well compared to other synthesis methods. Fig. 9 shows the boxplots for the user perception ratings for each model. It can be seen from Fig. 9 that the real samples were consistently perceived more perceptually plausible than both synthesis methods. There is very little difference between the physical model and alternative synthesis methods.

We perform one-way ANOVAs to determine the impact of synthesis method on the user authenticity ratings in each synthesis method case. In all three cases we identified a significant difference, see Table 5 (Harp, $F(2,765) = 110.6$, $p < 0.0001$, Propeller, $F(2,127) = 50.5$, $p < 0.0001$, Sword, $F(2,222) = 15.3713$, $p < 0.0001$).

In all cases our method was significantly worse than a recorded sample, as is the compared alternative synthesis method. It can be seen that for both the propeller and the sword models, that our method was significantly different from the comparison synthesis method. The box plots show that our method performed significantly better than the alternative synthesis method. The same cannot be said for the harp model and as such our method was "as plausible" as the alternative synthesis method.

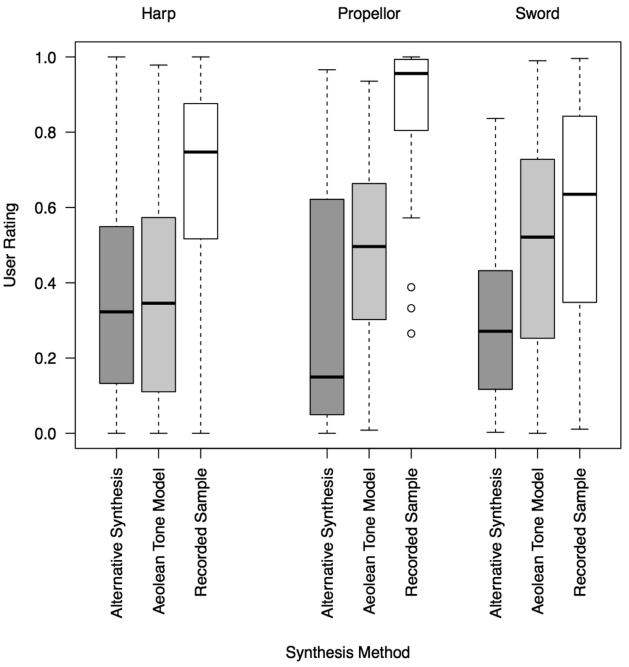

Fig. 9. Boxplots for all three synthesis models

Table 5. One-way ANOVAs for the different synthesis models perceptual ratings (**** = p<0.0001, *** = p<0.001, ** = p<0.01, * = p<0.05, - = p≥0.05)

		Aeolian	Alternative	Sample
	Aeolian	.	–	****
Harp	Alternative		.	****
	Sample			.
	Aeolian	.	*	****
Propeller	Alternative		.	****
	Sample			.
	Aeolian	.	**	**
Sword	Alternative		.	****
	Sample			.

6 DISCUSSION

A novel method for synthesizing aeroacoustic sounds has been undertaken by creating a compact sound source model and using this to build synthesis models based on the behavior of the various objects as well as additional fluid dynamics and mechanical properties. As shown in Fig. 1 there is a variety of fluid dynamics processes that generate fundamental sounds in which further objects can be derived. We recognize that larger objects, like high speed trains, will have a variety of different sources all generating sounds at the same time.

Semi-empirical equations have been used to identify sources of aeroacoustic noise in order for engineers to minimize noise pollution or structural fatigue, yet these equations give us a unique opportunity to make real-time sound synthesis models based on an accurate physical description of the objects we aim to replicate. Since properties like air density, air viscosity, speed of sound, etc., were integral to the model we are able to adapt the sound effects for evolving atmospheres.

The semi-empirical equations are defined and derived with assumptions and generalizations, often from the fundamental Navier-Stokes equations, to predict the aeroacoustic sound produced. It can be seen from the results presented in Table 4 and Fig. 6 that any assumptions made do not have a detrimental effect on these results. It is known that predicting fluid dynamics responses is nontrivial as evidenced by the difference in measured results from wind tunnel experiments to those obtained through CFD techniques. Even wind tunnel experiments themselves cannot be considered as a ground truth as there may be interference from instrumentation or indeed the tunnel itself.

In Sec. 3.5 we indicate that the ratio between the Aeolian tone dipoles and the wake quadrupoles had to be set perceptually. The value for this was not forthcoming from the literature and this is the only perceptual value given in the implementation. An exact relationship between the two would increase accuracy of our model and is an area for future developments.

The assumption made by [47] to neglect the exponential component in Eq. (6) is valid for low Mach numbers like that of wind (approx. 1% for $M = 0.02$) but incurs errors when Mach numbers increase (approx. 12% for $M = 0.06$). It is envisaged that future developments will benefit from inclusion of this factor. Similarly, the value for κ in Eq. (6) is expected to increase with higher Reynolds number, yielding $\kappa = 2$ for supercritical flow (i.e., the boundary layer on the cylinder becomes turbulent as well as the wake, $R_e > 5\text{x}10^6$). The introduction of this relationship, along with the additional factor in Eq. (6) may increase the accuracy of our model.

The objective evaluations of the Aeolian harp and propeller model indicated that our physical model does replicate the central sound generating properties but there are still additional properties that were missing. This may be because *thickness noise* or another noise source was missing from the propeller model (see [57]). There may be other fluid dynamic interactions that are not captured by the semi-empirical equations or other mechanical interactions not replicated by our models. Having exact measurements from swords, Aeolian harps, and propellers would assist in understanding what properties are not captured by our model. The preferred method for collecting real data would be in wind tunnel experiments which, due to time and availability, was not possible.

Perceptually, it was found our models produced sounds that were not as plausible as pre-recorded samples. A possible reason for the poor rating of the physical models compared to the actual recordings could be that the participants had preconceived beliefs for what each object should sound like. It is stated that memory plays an important role in perception [61] and if participants have heard a Foley sound effect for a sword more often than an actual sword sound, this may influence their perception of the physical model. In contrast, it can be argued that participants will have more likely heard the actual sounds of a golf club or baseball bat at live sporting events or within sporting broadcasts and hence their memory of these sounds would be closer to the physical model.

It would be of interest to carry out the perceptual evaluation with the sound effects played in context with an animation, similar to those presented in [21, 22]. In recent listening tests participants indicated that a combined audio-visual stimulus would be preferred over audio on its own. It is also noted that it is rare that these sound effects would be heard in isolation. Similar to adding the engine noise to the propeller model, additional sound sources may be present when the sounds occur naturally. These may be other aeroacoustic sounds like cavities for aircraft, impact sounds for swords or general environmental sounds for Aeolian harps. Our sound effects were all anechoic chamber versions of the sounds and therefore may be perceived as unnatural.

An increase in authenticity may be achieved with improvements to the behavior models of the different sound effects, especially the sword and propeller. For example, the sword swing behavior in our model is a perfect circle linearly accelerating and decelerating. In reality, the real swing of a sword will be in more of an arc with the elbow joint extending and retracting. A solution to this would be to attach the sound effect to a virtual object in a game engine allowing the motion to be controlled by the same physics controlling the graphics. This is similar for the propeller powered aircraft, which did not include banking, diving, and the effects of gravity on the power required when ascending in our listening test.

The models performed equally well as those created through other synthesis techniques; SMS for the Aeolian harp and propeller; CFD techniques, and a granular / additional synthesis technique for the sword. Not all of these techniques allow real-time sound production. Hence our model would be far more suited to an adaptive environment and give a more realistic acoustic response.

A further advantage of our model is the ability to extract the physical dimensions of an object or objects and map these directly into the sound effect models. This has particular attraction for environments using a physics engine where the details are already programmed into the system. The sound effects will react in harmony to changes within the game.

Standard Pure Data vanilla objects were chosen for the implementation. This ensured the open source nature of the sound effects as well as the ability to be implemented directly into a game engine. Future developments could include porting models into a language such as C++ where it is envisaged large computational savings can be made. The computational savings could then allow an increase in the number of compact sound sources used in each model or to decrease the number of assumptions made within the semi-empirical equations.

7 ACKNOWLEDGMENT

Thanks to Xiaolong Tang for assistance with computational calculations. Work supported by EPSRC

EP/G03723X/1. Professor Gurr's work can be found on his homepage[8].

8 REFERENCES

[1] H. H. Heller, D. G. Holmes, and E. E. Covert, "Flow-Induced Pressure Oscillations in Shallow Cavities," *Journal of Sound and Vibration*, 18, (1971). doi = 10.1016/0022-460X(71)90105-2.

[2] M. J. Lighthill "Sound Generated Aerodynamically," *Proceedings of the Royal Society of London A: Mathematical, Physical and Engineering Sciences*, vol. 267, (1962).

[3] N. Curle, "The Influence of Solid Boundaries upon Aerodynamic Sound," *Proceedings of the Royal Society of London A: Mathematical, Physical and Engineering Sciences* (1955). doi = 10.1098/rspa.1955.0191.

[4] D. G. Crighton et al., *Modern Methods in Analytical Acoustics: Lecture Notes* (Springer Science &; Business Media, 2012). doi = 10.1007/978-1-4471-0399-8.

[5] A. Farnell "An Introduction to Procedural Audio and its Application in Computer Games," *Audio Mostly Conference* (2007).

[6] R. Selfridge et al., "Physically Derived Synthesis Model of an Aeolian Tone," presented at the *141st Convention of the Audio Engineering Society* (2016 Sep.), convention paper 9679.

[7] A. Farnell *Designing Sound* (MIT Press Cambridge, 2010).

[8] C. Verron and G. Drettakis "Procedural Audio Modeling for Particle-Based Environmental Effects," presented at the *133rd Convention of the Audio Engineering Society* (2012 Oct.), convention paper 8764.

[9] C. Y. Loh and P. C. E Jorgenson "Computation of Tone Noises Generated in Viscous Flows," *Proceedings of the 4th CAA Workshop on Benchmark Problems, NASA/CP-2004-212954* (2004).

[10] Y. Dobashi, T. Yamamoto, and T. Nishita, "Real-Time Rendering of Aerodynamic Sound Using Sound Textures Based on Computational Fluid Dynamics," *ACM Transactions on Graphics* (2003). doi = 10.1145/882262.882339.

[11] N. Böttcher and S. Serafin "Design and Evaluation of Physically Inspired Models of Sound Effects in Computer Games," presented at the *AES 35th International Conference: Audio for Games* (2009 Feb.), conference paper 13.

[12] C. Heinrichs, A. McPherson, and A. Farnell, "Human Performance of Computational Sound Models for Immersive Environments," *The New Soundtrack*, 4, (2014). doi = 10.3366/sound.2014.0059.

[13] N. Böttcher, H. P. Martínez, and S. Serafin, "Procedural Audio in Computer Games Using Motion Controllers: An Evaluation on the Effect and Perception," *International Journal of Computer Games Technology*, 2013, (2013). doi = 10.1155/2013/371374.

[14] G. Korvel, V. Šimonyte, and V. Slivinskas, "A Modified Additive Synthesis Method Using Source-Filter Model," *Journal of the Audio Engineering Society*, 63, (2015). doi = 10.17743/jaes.2015.0055.

[15] M. Cardle et al., "Sound-by-Numbers: Motion-Driven Sound Synthesis," *Proceedings of the ACM SIGGRAPH* (2003).

[16] C. Schreck et al., "Real-Time Sound Synthesis for Paper Material Based on Geometric Analysis," *ACM SIGGRAPH Symposium on Computer Animation* (2016).

[17] A. Franck and V. Välimäki "Higher-Order Integrated Wavetable and Sampling Synthesis," *Journal of the Audio Engineering Society*, 61, (2013).

[18] V. Välimäki et al., "Physical Modeling of Plucked String Instruments with Application to Real-Time Sound Synthesis," *Journal of the Audio Engineering Society*, 44, (1996).

[19] J.-M. Adrien "The Missing Link: Modal Synthesis," in *Representations of Musical Signals* (MIT Press, 1991).

[20] J. D. Morrison and J.-M. Adrien, "Mosaic: A Framework for Modal Synthesis," *Computer Music Journal*, 17, (1993). doi = 10.2307/3680569.

[21] T. R. Langlois et al., "Eigenmode Compression for Modal Sound Models," ACM Transactions on Graphics (2014). doi = 10.1145/2601097.

[22] T. R. Langlois, C. Zheng, and D. L. James, "Toward Animating Water with Complex Acoustic Bubbles," *ACM Transactions on Graphics*, 35, (2016). doi = 10.1145/2897824.2925904.

[23] D. A. Jaffe and J. O. Smith, "Extensions of the Karplus-Strong Plucked-String Algorithm," *Computer Music Journal*, 7, (1983). doi = 10.2307/3680063.

[24] S. Ystad "Sound Modeling Applied to Flute Sounds," *Journal of the Audio Engineering Society*, 48, (2000).

[25] S. Kim, M. Kim, and W. S. Yeo "Digital Waveguide Synthesis of the Geomungo with a Time-Varying Loss Filter," *Journal of the Audio Engineering Society*, 61, (2013).

[26] S. Bilbao and A. Torin, "Numerical Modeling and Sound Synthesis for Articulated String/Fretboard Interactions," *Journal of the Audio Engineering Society*, 63, (2015). doi = 10.17743/jaes.2015.0023.

[27] N. Giordano, "Direct Numerical Simulation of a Recorder," *The Journal of the Acoustical Society of America*, 133, (2013). doi = 10.1121/1.4773268.

[28] N. Giordano, "Simulation Studies of a Recorder in Three Dimensions," *The Journal of the Acoustical Society of America*, 135, (2014). doi = 10.1121/1.4861249.

[29] N. Giordano, "Computational Study of the Piccolo: Evidence for Chaotic Tones," *The Journal of the Acoustical Society of America*, 140, (2016). doi = 10.1121/1.4962632.

[30] S. Bilbao and B. Hamilton, "Wave-Based Room Acoustics Simulation: Explicit/Implicit Finite Volume Modeling of Viscothermal Losses and Frequency-Dependent Boundaries," *Journal of the Audio Engineering Society*, 65, (2017). doi = 10.17743/jaes.2016.0057

[8] http://web.usca.edu/math/faculty-sites/henry-gurr/aeolian.dot

[31] S. Bilbao and C. J. Webb "Physical Modeling of Timpani Drums in 3d on GPGPUs," *Journal of the Audio Engineering Society*, 61, (2013).

[32] A. Allen and N. Raghuvanshi, "Aerophones in Flatland: Interactive Wave Simulation of Wind Instruments," *ACM Transactions on Graphics*, 34, (2015). doi = 10.1145/2767001.

[33] V. Zappi et al., "Towards Real-Time Two-Dimensional Wave Propagation for Articulatory Speech Synthesis," *Proceedings of Meetings on Acoustics 171 ASA*, volume 26 (2016). doi = 10.1121/2.0000395.

[34] E. Motuk, R. Woods, and S. Bilbao, "Implementation of Finite Difference Schemes for the Wave Equation on FPGA," *Acoustics, Speech, and Signal Processing. Proceedings. IEEE International Conference on*, volume 3 (2005). doi = 10.1109/ICASSP.2005.1415690.

[35] F. Pfeifle and R. Bader, "Real-Time Finite-Difference Method Pphysical Modeling of Musical Instruments Using Field-Programmable Gate Array Hardware," *Journal of the Audio Engineering Society*, 63, (2016). doi = 10.17743/jaes.2015.0089.

[36] C. Cheong et al., "Computation of Aeolian Tone from a Circular Cylinder Using Source Models," *Applied Acoustics*, 69, (2008). doi = 10.1016/j.apacoust.2006.10.004.

[37] U. Fey, M. König, and H. Eckelmann, "A New Strouhal-Reynolds-Number Relationship for the Circular Cylinder in the Range 47 to 200000," *Physics of Fluids*, 10, (1998). doi = 10.1063/1.869675.

[38] H. Fujita, "The Characteristics of the Aeolian Tone Radiated from Two-Dimensional Cylinders," *Fluid Dynamics Research*, 42, (2010). doi = 10.1088/0169-5983/42/1/015002.

[39] J. E. Ffowcs Williams and D. L. Hawkings, "Sound Generation by Turbulence and Surfaces in Arbitrary Motion," Philosophical Transactions of the Royal Society of London A: Mathematical, Physical and Engineering Sciences, (1969). doi = 10.1098/rsta.1969.0031.

[40] M. E. Goldstein, *Aeroacoustics* (McGraw-Hill International Book Co., New York, 1976).

[41] B. Etkin, G. K. Korbacher, and R. T. Keefe, "Acoustic Radiation from a Stationary Cylinder in a Fluid Stream (Aeolian Tones)," *Journal of the Acoustical Society of America*, 29, (1957). doi = 10.1121/1.1905104.

[42] J. C. Hardin and S. L. Lamkin, "Aeroacoustic Computation of Cylinder Wake Flow," *AIAA journal*, 22, (1984). doi = 10.2514/3.48418.

[43] C. Norberg, *Effects of Reynolds Number and a Low-Intensity Freestream Turbulence on the Flow around a Circular Cylinder* (Chalmers University, Goteborg, Sweden, Technological Publications, 1987).

[44] A. Powell, "Similarity and Turbulent Jet Noise," *The Journal of the Acoustical Society of America*, 31, (1959). doi = 10.1121/1.1907792.

[45] R. E. Musafir "On the Sound Field of Organized Vorticity in Jet Flows," *13th International Congress on Acoustics* (1989).

[46] E. J. Avital, M. Alonso, and V. Supontisky, "Computational Aeroacoustics: The Low Speed Jet," *The Aeronautical Journal*, 112, (2008). doi = 10.1017/s0001924000002360.

[47] O. M. Phillips, "The Intensity of Aeolian Tones," *Journal of Fluid Mechanics*, (1956). doi = 10.1017/s0022112056000408.

[48] C. Norberg, "Flow around a Circular Cylinder: Aspects of Fluctuating Lift," *Journal of Fluids and Structures*, 15, (2001). doi = 10.1006/jfls.2000.0367.

[49] N. J. Kasdin, "Discrete Simulation of Colored Noise and Stochastic Processes and 1/f α Power Law Noise Generation," *Proceedings of the IEEE*, 83, (1995). doi = 10.1109/5.381848.

[50] L. A. Bazhenova and A. G. Semenov, "Nature of the Source of Vortex Sound Flowing around a Cylindrical Profile," *Acoustical Physics*, 60, (2014). doi = 10.1134/s1063771014060037.

[51] T. Uda et al., "Cross-Correlation Analysis of Aeroacoustic Sound and Flow Field Using Time-Resolved PIV," *Proceedings of 15th Int. Symp. on Application of Laser Techniques to Fluid Mechanics* (2010).

[52] C. K. W. Tam and J. C. Hardin *Second Computational Aeroacoustics (CAA): Workshop on Benchmark Problems* (NASA, 1997).

[53] J. H. Gerrard, "An Experimental Investigation of the Oscillating Lift and Drag of a Circular Cylinder Shedding Turbulent Vortices," *Journal of Fluid Mechanics*, 11, (1961). doi = 10.1017/s0022112061000494.

[54] R. Selfridge, D. Moffat, and J. D. Reiss, "Real-Time Physical Model for Synthesis of Sword Swing Sounds," Sound and Music Computing, (2017).

[55] R. Selfridge et al., "Real-Time Physical Model of an Aeolian Harp," *24th International Congress on Sound and Vibration* (2017).

[56] R. Selfridge, D. Moffat, and J. D. Reiss, "Physically Derived Sound Synthesis Model of a Propeller," *Audio Mostly Conference* (2017). doi = 10.1145/3123514.3123524.

[57] J. E. Marte and D. W. Kurtz *A Review of Aerodynamic Noise from Propellers, Rotors, and Lift Fans* (Jet Propulsion Laboratory, California Institute of Technology, 1970).

[58] X. Amatriain et al., "Spectral Processing," *Proc. Int. Conf. on Digital Audio Effects* (2002). doi = 10.1002/0470846046.ch10.

[59] N. Jillings et al., "Web Audio Evaluation Tool: A Browser-Based Listening Test Environment," Sound and Music Computing, (2015).

[60] Recommendation ITU-R BS.1534-3, "Method for the subjective assessment of intermediate quality level of audio systems," *International Telecommunication Union Radiocommunication Assembly* (2015).

[61] W. W. Gaver and D. A. Norman *Everyday Listening and Auditory Icons,* Ph.D. thesis, University of California, San Diego, Department of Cognitive Science and Psychology (1988).

APPENDIX A

Coefficient values for bandpass filter given in Eq. (17) in terms of f, which is substituted for the tone frequency we are aiming to model, are given below.

$$\beta_1 = (2 - p_1 - p_2)^2$$

$$\beta_2 = 2(2 - p_1 - p_2)(2p_1p_2 - p_1 - p_2)$$

$$\beta_3 = (2p_1p_2 - p_1 - p_2)^2$$

$$\alpha_1 = 2(p_1 + p_2)$$

$$\alpha_2 = 2(p_1p_2) + (p_1 + p_2)^2$$

$$\alpha_3 = 2(p_1 + p_2)(p_1p_2)$$

$$\alpha_4 = (p_1p_2)^2$$

$$p_1 = \left(1 - \frac{f/Q}{f_s}\right)\left(\cos 2\pi\frac{f}{f_s} + i \sin 2\pi\frac{f}{f_s}\right)$$

$$p_1 = \left(1 - \frac{f/Q}{f_s}\right)\left(\cos 2\pi\frac{f}{f_s} - i \sin 2\pi\frac{f}{f_s}\right)$$

THE AUTHORS

Rod Selfridge

David Moffat

Eldad J. Avital

Joshua D. Reiss

Rod Selfridge is a Ph.D. researcher within the Media and Arts Technology Doctoral College at Queen Mary University of London. In 1995 Rod graduated from Edinburgh Napier University in electronics and communication engineering and worked as an offshore engineer before moving on to a non-technical role. In 2011 he completed a Masters with Distinction in digital music processing at Queen Mary University of London. In 2014 Rod worked with BBC Research and Development for six months as part of the Ph.D. program.

•

David Moffat is a Ph.D. researcher at Queen Mary University of London working within the sound synthesis research team, focused on perceptual evaluation of synthesized sound effects. His research evaluates current state of the art in sound synthesis and aims to objectively identify what makes a particular sound effect realistic. Research interests include sound synthesis; procedural audio; audio production technology; real time and live mixing tools, and DSP; perceptive, qualitative, and objective measures; and metrics for the evaluation of audio technologies. David received his M.Sc. from Queen Mary University of London in 2014.

Dr. Eldad J. Avital is a Reader in computational fluids and acoustics with the School of Engineering and Materials Science. His expertise is in fluid dynamics and acoustics, specializing in computational aero-acoustics, aerodynamics and hydrodynamics, fluids-structure interaction, and bio-fluids. Dr. Avital is a Fellow of the UK Higher Education Academy, Senior member AIAA, and a member in EuroMech.

•

Prof. Josh Reiss is a Professor of audio engineering with the Centre for Digital Music at Queen Mary University of London. He received his Ph.D. in physics from Georgia Tech, specializing in analysis of nonlinear systems. Prof. Reiss has published over 100 scientific papers and serves on several steering and technical committees. He has investigated music retrieval systems, time scaling and pitch shifting techniques, polyphonic music transcription, loudspeaker design, automatic mixing for live sound and digital audio effects, among others. His primary focus of research, which ties together many of the above topics, is on the use of state-of-the-art signal processing techniques for professional sound engineering.